Photo-Injection p-i-n Diode Switch for High-Power RF Switching

E. W. Jacobs, D. W. Fogliatti, H. Nguyen, D. J. Albares, C. T. Chang, *Member, IEEE*, and C. K. Sun

***Abstract*—The high RF power-switching properties of the photo-injection p-i-n switch (PIPINS), an optically controlled RF switch, are investigated. Proper functioning of a PIPINS as a low insertion-loss RF switch requires that it operates as a photoconductor, where the photo-injected charge is much greater than the RF sweep out charge. Insertion loss using 650-mW optical power was <0.4 dB at RF (VHF–UHF) power in excess of 200 W, and devices successfully standoff 200-W incident RF power with the series isolation being determined by the device capacitance (e.g., 225 fF). PIPINS hot-switching measurements are reported for the first time, with output RF power up to 180 W at low duty cycle, rise times of 1 μs, and fall times for a series shunt switch of $\approx$2.5 μs. The RF power for hot switching a PIPINS is limited by a latch-on effect, which is dependent on a variety of parameters, including duty cycle and repetition period, consistent with thermally generated carriers contributing to the latch-on effect. The switching properties of PIPINS make them a candidate for high RF power applications such as reconfigurable antennas, where electromagnetic isolation of the switch and control lines are critical.**

***Index Terms*—Optical switches, optolectronic devices, RF diodes, RF switches.**

I. Introduction

OPTICALLY controlled electrical switches are of interest for applications that require electromagnetically isolated control. In addition to electromagnetic isolation, optoelectronic (OE) RF semiconductor switches possess switching times and reliability of semiconductor RF switches, and are controlled via lightweight low-loss optical fiber, thereby making them well suited to applications of reconfiguring antenna radiating elements, feeds, and tuning circuits [1], [2]. In this paper, high RF power-switching properties of the photo-injection p-i-n switch (PIPINS) [3] are reported for both cold and hot switching.

RF switching applications generally require low on-resistance ($R_{\rm on} \leq 5\ \Omega$), low capacitance for high-frequency isolation, and a minimum of optical control power. Switching time requirements can vary from milliseconds to nanoseconds, and RF power requirements vary up to kilowatts. Several OE RF switch configurations have been demonstrated, which meet some subset of these requirements. These devices include photoconductors, phototransistors, surface-depleted optical FETs [4], photovoltaically biased FET (PV-FET) switches [4], [5], electrically biased p-i-n diode switches [6], photovoltaically biased p-i-n diode (PV-PIN) switches [7], and the PIPINS [3]. The performance characteristics of these optically controlled semiconductor switches are generally similar to their electrically controlled counterparts, where some performance improvement is gained by the optically isolated control. The FET-based OE switches are limited to switching only a few watts of RF power, though they have the advantage of requiring little ($\ll$1 mW) optical control power. Compound FET switches where the RF voltage swing is distributed across several FETs in series enables significantly increased RF power capability [8], though no optically controlled version of this type of device has been reported. The PV-FET and PV-PIN use indirect optical control wherein photovoltaic cells located near the switching elements provide charge to the switching elements via isolating chokes or resistors. PV-PINs can be expected to handle more RF power (>100 W) than the PV-FET at the cost of increased optical power, e.g., in [7], a series switch with $P_{\rm rf} = 25$ W, $P_o = 200$ mW, and $R_{\rm on} = 3\,\Omega$ was demonstrated.

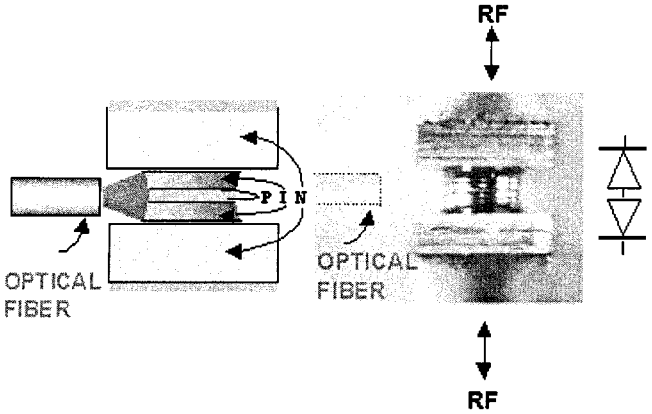

Fig. 1. Schematic, photograph, and circuit representation of a PIPINS.

The PIPINS, shown in Fig. 1, is a back-to-back p-i-n diode configuration where direct optical injection creates electron hole pairs in the intrinsic region of the p-i-n diodes, producing the on state. In the absence of optical illumination, the back-to-back diodes provide the reflective off state, where the series capacitance of the diodes determines the switch isolation. The PIPINS requires no dc biasing, the direct optical injection eliminates the need for chokes and/or resistors that are required by OE designs such as PV-PIN and PV-FET switches, and the optical-to-electrical conversion efficiency is greater than that of the PV-PIN.

Manuscript received October 10, 2000; revised March 2, 2001. This work was supported by W. Bratt, SPAWAR PMW-163, San Diego, CA.

E. W. Jacobs, D. W. Fogliatti, and H. Nguyen are with Code D825, Space and Naval Warfare Systems Center San Diego, San Diego, CA 92152-5001 USA (e-mail: jacobs@nosc.mil).

D. J. Albares was with Code D825, Space and Naval Warfare Systems Center San Diego, San Diego, CA 92152-5001 USA. He is now with the Peregrine Semiconductor Corporation, San Diego, CA 92121 USA.

C. T. Chang is with the Department of Electrical and Computer Engineering, San Diego State University, San Diego, CA 92182 USA.

C. K. Sun was with Code D825, Space and Naval Warfare Systems Center San Diego, San Diego, CA 92152-5001 USA. He is now with Lightwave Solutions Inc., San Diego, CA 92126 USA.

Publisher Item Identifier S 0018-9480(02)01152-3.

These properties make the PIPINS particularly attractive for antenna applications such as reconfigurable antennas [2]. Electromagnetically transparent optical fibers would deliver control signals from remote laser sources to PIPINS positioned on the antenna structure. With selective switching of the PIPINS, antenna length or shape could be adjusted to improved wide-band performance, or different antenna elements within the same foot print could be activated or made transparent. Small inductors connected in parallel with the PIPINS forming a tuned *LC* circuit could be employed to increase switch isolation over a specific frequency range.

In [3], PIPINS broad-band insertion-loss data at low RF power, and insertion-loss data between 300–400 MHz up to 20-W RF power was reported. For transmitting and jamming applications, higher RF power properties of the switch become important. In this paper, insertion loss (IL) and standoff measurements are performed in excess of 200-W RF power; this power being limited by the power amplifier instrumentation. This was achieved with 650-mW optical control power, representing a significant gain as defined by the ratio of the switched RF power to the optical control power. In addition, "hot" switching (where the device is switched in the presence of the RF signal) properties of the PIPINS, are reported for the first time.

II. Measurements

The PIPINS devices were made, as shown in Fig. 1, by soldering together the P contacts of two mesa-type silicon p-i-n diodes.[1] The epitaxially grown intrinsic layer (carrier concentration $\approx 10^{12}/\text{cm}^3$) was either 50- or 100-$\mu$m thick, depending on the device, and the mesa diameter was 760 μm. The N-type die was square, 914 μm on a side, with carrier concentration $\approx 6 \times 10^{19}/\text{cm}^3$. The P-layer doping concentration was $\approx 8 \times 10^{19}/\text{cm}^3$, where the P-layer thickness was ≈ 4 μm and the doping profile from the P region to the I region was a step $\approx$3-μm wide. The reverse bias leakage current of the diodes was low (<1 μA) and the forward bias (>80 mA) resistance was 1 Ω measured at 100 MHz. The dc reverse bias break down for 50-μm intrinsic layer diodes was $\approx$350 V, and for 100-μm intrinsic layer diodes $\approx$450 V. For the 50-μm intrinsic layer diodes, $C \simeq 700$ fF, and for the 100-μm intrinsic layer diodes, $C \simeq 450$ fF, both measured at 100 MHz. The PIPINS were mounted on 50-Ω microstrip transmission lines on aluminum–nitrite substrates. The substrates were attached with silver epoxy to brass fixtures with SMA flange-mount tab connectors.

The PIPINS were characterized for conversion efficiency of photons to charge carriers, the isolation at low RF power as a function of frequency, and the low RF power IL as a function of frequency and optical power. The conversion efficiency for a p-i-n diode under high reverse dc bias is given by $\eta_t = (I_p/q)/(P_o/(h\nu)) = (I_p/P_o) \times 1.24/\lambda$, where I_p is the photocurrent, P_o is the optical power out of the fiber, and λ is the wavelength of light measured in micrometers [9]. For the measurements in this paper, $\lambda = 0.81$ μm, and the optical fiber had a 100-μm core with NA $= 0.36$. By the definition used here, η_t accounts for the quantum efficiency of the device and the optical coupling efficiency from the optical fiber to the device. Due to the back-to-back p-i-n diode configuration of the PIPINS, the dc photocurrent I_p was measured as follows. First, the fiber was positioned to minimize the RF IL. Measurements were not sensitive to slightly increasing the distance from the end of the fiber to the device, even for the case of the thinner $t_i = 100$ μm devices. The RF source was then removed, the PIPINS was dc biased in each direction, and the dc photocurrents in each direction were added. The bias voltage was 30 V, which provided an electric field well in excess of that needed to saturate the measured I_p for even the highest P_o. The resulting plot of conversion efficiency as a function of optical power out of the fiber is shown in Fig. 2. The mean and standard deviation of η_t are shown for three PIPINS with total intrinsic region thickness $t_i = 100$ μm, and five PIPINS with $t_i = 200$ μm. The decrease in η_t as P_o increases can be attributed to increased recombination due to the high density of charge carriers. The low optical power values of η_t in Fig. 2 correspond to a responsivity $I_p/P_o \simeq 0.5$ A/W, a typical value for p-i-n photodetectors.

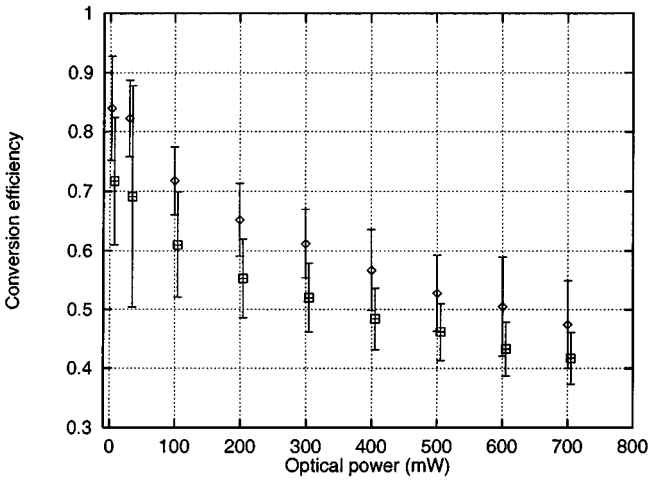

Fig. 2. Optical conversion efficiency as a function of P_o. The mean and standard deviation for measurement of five PIPINS with $t_i = 200$ μm (□), and three PIPINS with $t_i = 100$ μm (◇) are shown. The $t_i = 200$ μm data points are shifted to 5 mW larger P_o for clarity.

Figs. 3 and 4 show low RF power (0 dBm) isolation and IL data for a series PIPINS, as measured with an HP8753C network analyzer. The $S21$ measurements were calibrated against an identical package with a straight through transmission line. The $S21$ data in Figs. 3 and 4 is shown for a PIPINS with $t_i = 100$ μm, and a PIPINS with $t_i = 200$ μm. At the high-frequency end of this data, the capacitance and the off-state series resistance (at the interfaces of the intrinsic and doped regions) contribute to the isolation of the device. A capacitance of 380 fF for the $t_i = 100$ μm PIPINS, and 225 fF for the $t_i = 200$ μm PIPINS, with a series resistance of 100 Ω yields a reasonable fit to this data.

The IL data in Fig. 4 is also shown as a function of P_o. Measurements on these devices at higher frequency shows that the IL remains essentially flat up to at least 6 GHz. The increased ripple in the data as P_o decreases is due to reflections at the

[1]The diodes used in these experiments were custom made by the Metelics Corporation, Sunnyvale, CA.

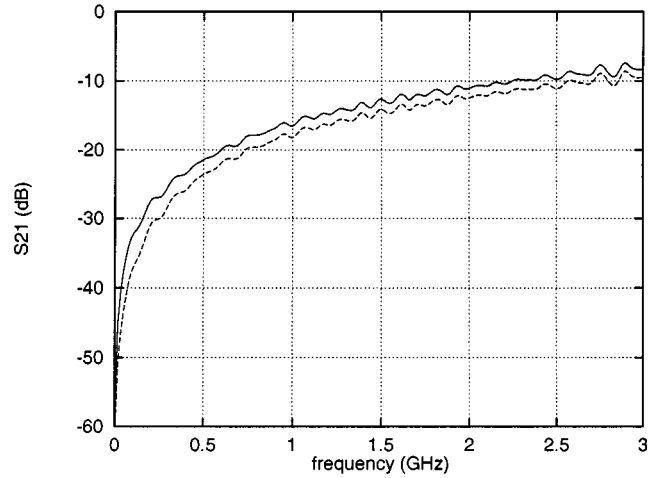

Fig. 3. Isolation as a function of frequency with $P_{\rm rf} = 0$ dBm, where the upper curve is for a PIPINS with $t_i = 100$ μm, and the lower curve is for a PIPINS made with $t_i = 200$ μm.

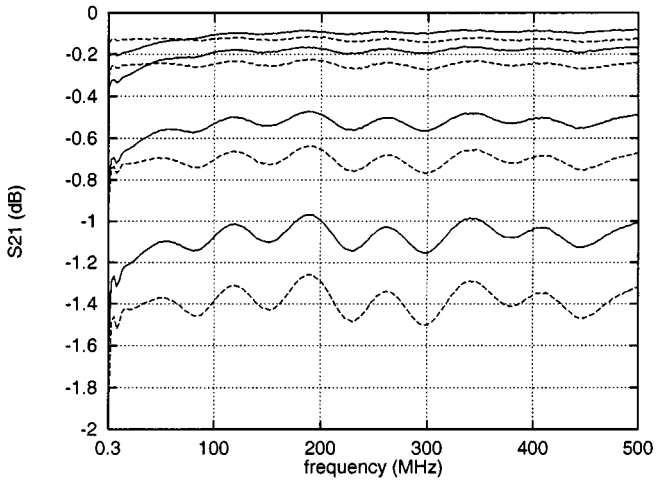

Fig. 4. IL as a function of frequency for PIPINS with $t_i = 100$ μm (solid lines) and 200 μm (dashed lines) with $P_{\rm rf} = 0$ dBm and P_o as a parameter. In increasing order of IL P_o was 706, 166, 15.3, and 2.3 mW.

PIPINS caused by impedance mismatch, the shape of the ripples being highly dependent on the cable lengths employed.

High RF power IL measurements are shown in Fig. 5. The RF signal was provided to the PIPINS by an HP8645A signal generator driving an Ophir GRF5041 RF (200-W power) amplifier. The signal was attenuated after the PIPINS (with attenuators rated at 1000 W to minimize error caused by the change in attenuation due to heating) before the RF power was measured with an HP 436A RF power meter. As with the low power measurements, the high RF power measurements were calibrated against a package identical to the PIPINS package, but with a straight through transmission line. This data was taken with a $t_i = 200$ μm PIPINS (as were the remainder of the data in this paper) with $f = 30, 88$, and 333 MHz and $P_o = 650$ mW. The maximum RF power levels measured were limited by the RF power amplifier. Systematic mean time to failure data for PIPINS in continuous on state was not undertaken in this study, though no failures were observed for PIPINS at the maximum attainable RF power levels wherein devices were routinely in this state for 5–10 min.

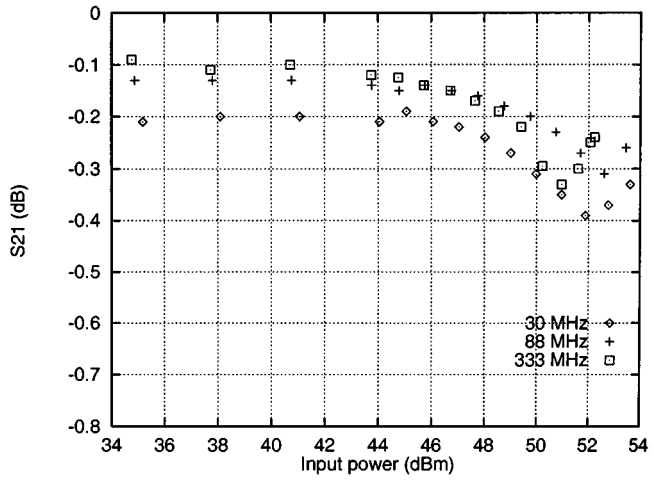

Fig. 5. High RF power IL data with $P_o = 650$ mW.

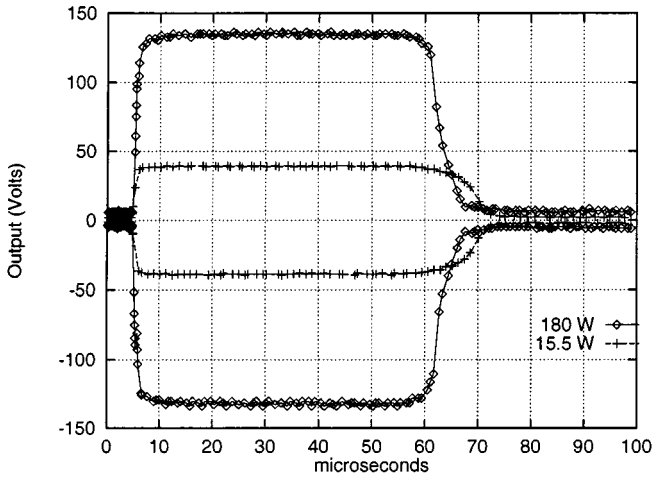

Fig. 6. RF envelope for hot-switched PIPINS with $P_o = 650$ mW, $f = 300$ MHz, $t_{\rm on} = 50$ μs, and $T = 30$ ms.

With the switch in the off state, RF standoff voltage measurements were performed. For these measurements, the reflected power was monitored (via the third port of the circulator located between the RF power amplifier and PIPINS), as was the signal capacitively coupled through the PIPINS. A PIPINS can exhibit self-turn-on, i.e., the PIPINS will switch from the off state to the on state in the absence of optical illumination at high enough incident RF power. Standoff measurements at 333 MHz were performed without self-turn-on, and were limited (by the RF amplifier and loss in the circulator) to 52.5-dBm incident RF power at the device-under-test for most measurements. In one case, this power was pushed to 200 W, also indicating no self-turn-on.

Applications where switching occurs only when the RF signal is off or at low power (cold switching) require specification of the steady-state IL and standoff measurements presented above. For applications that require switching in the presence of the high-power RF signal, the hot-switching properties of the switch must be understood. Hot switching requires reliability through the on–off transition states in the presence of the high-power signal, therefore, the hot-switching power capability of a switch is typically significantly less than indicated by steady-state IL and standoff measurements. Fig. 6

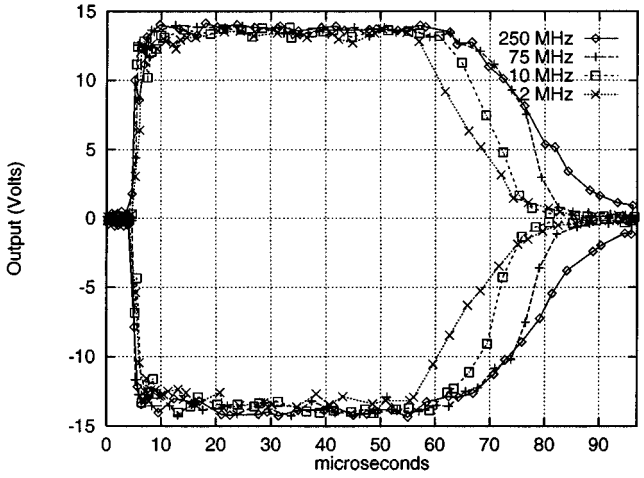

Fig. 7. RF envelope for hot-switched PIPINS as a function of frequency with $P_o = 650$ mW, $t_{\rm on} = 50$ μs $T = 5$ ms.

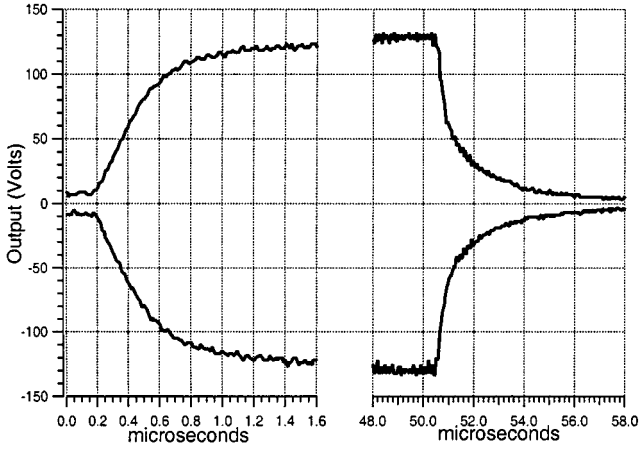

Fig. 8. RF envelope for a hot-switched series-shunt PIPINS with $P_o = 650$ mW to each PIPINS, $f = 333$ MHz, $t_{\rm on} = 50$ μs, and $T = 90$ ms.

shows data for a hot-switched PIPINS, where the envelope of the 300-MHz RF signal is plotted. The PIPINS was illuminated with $P_o = 650$ mW during the $t_{\rm on} = 50$ μs on period, and the repetition period was $T = 30$ ms. The output voltage was measured across 50 Ω, therefore the output power during the on state for this measurement was 180 W. Also shown in Fig. 6 is hot switching with 15.5-W output power during the on state.

The fall time of the series PIPINS RF envelope is governed by charge carrier sweep out and recombination in the PIPINS. As a result, in addition to being dependent on the material and geometric properties of the PIPINS, the fall time is also dependent on P_o, $P_{\rm rf}$, and RF frequency f. Fig. 7 shows hot switching as a function of f. The envelope of a $P_{\rm rf} = 2$ W signal at 2, 10, 75, and 250 MHz is shown. At 2 MHz, P_o is large enough to saturate the on-state IL, but immediately after $t_{\rm on} = 50$ μs, the signal amplitude starts dropping. The total fall time measured from the end of $t_{\rm on}$ is 22 μs for the 2-MHz case, and 37 μs when $f = 250$ MHz. A set of similar curves can be obtained as a function of $P_{\rm rf}$ (Fig. 6) and P_o, where the fall time decreases as a function of increasing $P_{\rm rf}$ and decreasing P_o.

The rise time of a series PIPINS follows the rise time of the optical control signal. The rise time of the optical control signal, as measured with a fast photodiode, was 0.5 μs, and its fall time was 0.2 μs. For applications where a fast fall time is required and where a ground plane is present, a series-shunt PIPINS circuit can be utilized, wherein the fast turn-on time of the shunt PIPINS is used to achieve a fast fall time for the switch. Fig. 8 focuses on the rising and falling edges of a hot-switched series-shunt PIPINS indicating a rise time of approximately 1 μs and a fall time of 2.5 μs. For this data, $P_o = 650$ mW, $t_{\rm on} = 50$ μs, $T = 90$ ms, and $P_{\rm rf} = 170$ W at the output.

The maximum $P_{\rm rf}$ that a PIPINS can handle in the hot-switched mode is limited by a latch-on effect, i.e., the switch remains in the on state after the optical control signal turns off. The RF power at latch-on ($P_{\rm latch}$) is dependent on several parameters. For example, Fig. 9 plots $P_{\rm latch}$ as a function of the repetition period T when the duty cycle $d = t_{\rm on}/T$ is 50%. Latch-on is also dependent on the duty cycle, as can be seen by comparing the data in Figs. 6 and 8 to that of Fig. 9. The duty cycle was considerably less than 50% in Figs. 6 and 8

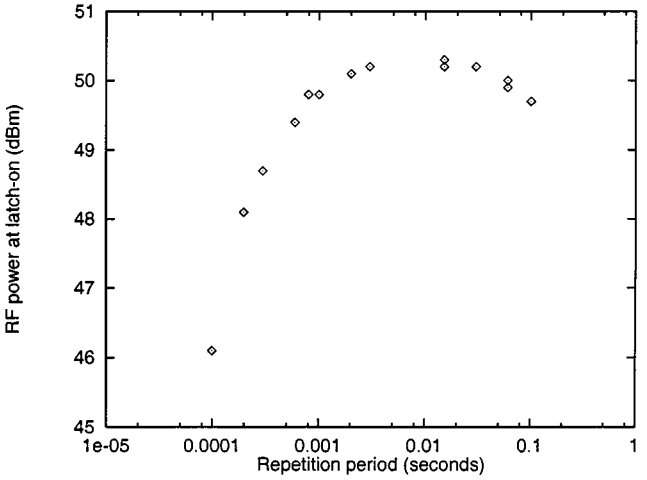

Fig. 9. RF power at latch-on with 50% duty cycle as a function of the repetition period with $P_o = 650$ mW and $f = 300$ MHz.

allowing for higher pulse power operation than the data shown in Fig. 9. The threshold for latch-on is abrupt as demonstrated in a measurement where a device was switched at $P_{\rm rf}$ 0.2 dB below $P_{\rm latch}$ for 30 min without latch-on ever occurring.

The linearity in the on state of the PIPINS was studied with two-tone intermodulation measurements with up to $P_{\rm rf} = 50$ W at each fundamental frequency. For the $t_i = 200$ μm PIPINS, with $P_{\rm rf} = 50$ W at each fundamental ($f_1 = 44$ MHz and $f_2 = 49$ MHz), the third-order intermodulation product at 54 MHz was 60 dB down from the fundamental.

III. Discussion

In this section, IL, rise and fall times, and latch-on of a PIPINS are discussed. The conduction in a PIPINS is governed by the storage and sweep out of the photo-generated charge carriers, and is dependent on the material and geometric properties of the diodes, and the operational parameters P_o, $P_{\rm rf}$, and f. The charge supplied to the diode by the control optical power P_o of wavelength λ (in micrometers) is

$$Q_p = I_p \tau = P_o \eta_t \tau q / h\nu = P_o \eta_t \lambda \tau / 1.24 \qquad (1)$$

where τ is the effective charge carrier lifetime. This can be compared to the charge modulation caused by the RF signal during half an RF cycle

$$Q_s = \int_0^{0.5/f} I_s \times \sin(2\pi f t)\, dt = \frac{I_s}{\pi f} = \frac{\sqrt{2P_{\rm rf}/Z_0}}{\pi f} \quad (2)$$

where I_s is the amplitude of the RF current. During half an RF cycle, the stored charge on the forward-biased diode will be increased due to carrier injection from the average value Q_p to $Q_p + Q_s/2$, while the charge on the reverse biased diode will be reduced to $Q_p - Q_s/2$ due to carrier sweep out. The IL of the PIPINS is determined by the less-conductive diode, therefore, $Q_p \gg Q_s/2$ is needed for low IL, and as $Q_s/2$ approaches Q_p, the PIPINS IL will increase. For a low RF frequency (or a dc bias) where $Q_p \gg Q_s/2$ is not satisfied, the PIPINS behaves like a reverse-biased p-i-n photodetector, the photocurrent being proportional to the optical power and insensitive to the reverse-biasing voltage and device thickness. This is the case for the measurement of η_t in Fig. 2, where it is seen that η_t was only weakly dependent on the t_i, and where the reverse bias of 30 V was well large enough to saturate the measurement of I_p.

When $Q_p \gg Q_s/2$, conduction in a PIPINS approximates that of a photoconductor. For a photoconductor,

$$R_{\rm on} = \frac{t_i^2}{Q_p \mu} + 2R_c \quad (3)$$

where μ is the sum of the electron and hole mobilities, and R_c is the contact resistance of a single diode. The IL as measured in Fig. 4 is related to $R_{\rm on}$ by

$$\text{IL} = 20 \times \log\left(1 + \frac{R_{\rm on}}{2Z_o}\right) \quad (4)$$

where $Z_0 = 50\ \Omega$. The PIPINS contact resistance $2R_c$ is the minimum $R_{\rm on}$ and is estimated to be $1\ \Omega$ from (4) and the lowest IL (0.09 dB) $P_o = 706$ mW curve in Fig. 4. The $P_o = 706$ mW curve for the $t_i = 200\ \mu$m PIPINS in Fig. 4 yields an estimation from (4) of $R_{\rm on} = 1.5\ \Omega$. The carrier lifetime for this case is estimated from (3) to be $\tau = 2.1\ \mu$s, where $\mu = 1830$ cm^2/Vs and $\eta_t = 0.45$ (from Fig. 2) are used. The value of τ is parameter dependent. For example, for larger volume to surface area devices, the lifetime is expected to increase due the reduced impact of surface recombination [10]. Also, as charge carrier density increases, the value of τ decreases [11]. Both these effects can be seen by calculating τ from (3) and (4) for the other curves in Fig. 4. In the discussion that follows, the estimate of $\tau = 2.1\ \mu$s is used to analyze Figs. 6–8 as $P_o = 650$ mW and $t_i = 200\ \mu$m for these data.

In order to operate a PIPINS properly as a low IL photoconductive switch, $Q_p \gg Q_s/2$ is needed for the less conductive diode under a RF reverse-bias half cycle. Making uses of (1) and (2), the photoconductive condition is rewritten as

$$2\pi f \tau \gg I_s/I_p. \quad (5)$$

Here, the ratio of RF current amplitude I_s to dc photocurrent I_p is defined as the current gain $G \equiv I_s/I_p$, and $\theta \equiv 2\pi f \tau$ is the RF phase angle over the carrier lifetime τ. Low PIPINS IL is associated with high θ/G or high $Q_p/(Q_s/2)$, or in terms of operational parameters, high P_o, high f, and low $P_{\rm rf}$. Similarly, high IL is expected with low P_o, low f, and high $P_{\rm rf}$, where RF carrier sweep out becomes appreciable.

The photocurrent is estimated to be $I_p \simeq 191$ mA for a PIPINS with $P_o = 650$ mW at $\lambda = 0.81\ \mu$m with a measured $\eta_t = 0.45$. The highest $P_{\rm rf}$ lowest f data in Fig. 5 has $P_{\rm rf} = 224$ W and $f = 30$ MHz, corresponding to a current gain of $G \simeq 16$ and a phase angle $\theta \simeq 396$ rad, or in terms of charge storage and sweep out, $Q_s/2 \simeq Q_p/25$. For the PIPINS hot-switching curve with lowest f in Fig. 7, $P_{\rm rf} = 2$ W, $f = 2$ MHz, and again, $P_o = 650$ mW, which corresponds to an estimate of $G \simeq 1.5$ and $\theta \simeq 26$. In terms of charge storage and sweep out, $Q_s/2 \simeq Q_p/18$. Therefore, this simple analysis is consistent with the measured low IL results.

In designing a PIPINS, high isolation, low IL, fast switching times, and high RF power capability are all desired properties. The underlying physical parameters dictate a compromise between these properties, e.g., increasing the device thickness improves isolation at the cost of IL, decreasing the device width improves isolation at the cost of power-handling capability, and decreasing the carrier lifetime improves the turn-off time at the cost of IL.

A. Rise and Fall Times

The rise time for a hot-switched PIPINS at $P_{\rm rf} = 170$ W, as shown in Fig. 8, is 1 μs. Since the *RC* device time constant is negligible, the transit time across the intrinsic region is fast, and the conductivity of the PIPINS is a function of the carrier concentration, which is dependent on P_o, the PIPINS rise time should be close to the rise time of the optical control signal. The rise time of the optical control signal, as measured with a fast response photo diode, was 0.5 μs.

There are two periods of the PIPINS total fall time, the first when the charge carrier concentration in the PIPINS is high enough that the contact resistance dominates $R_{\rm on}$. This period is essentially a turn-off delay time because, as seen in the higher frequency curves in Fig. 7, the RF signal remains close to full amplitude even after $t_{\rm on}$ has ended. The second period is when the charge carrier concentration has dropped enough that $R_{\rm on}$ is no longer dominated by the contact resistance, at which point the IL increases appreciably. In the following, the total fall time is measured from the time the light is turned off to 10% of the on-state RF amplitude. The fall time of the optical control signal was 0.2 μs, relatively fast as compared to τ, in which case the total fall time for a series PIPINS is a function of charge storage, sweep out, and recombination. From the previous discussion, the total fall time of a series PIPINS will decrease with increasing Q_s associated with high $P_{\rm rf}$ and low f, and decreasing Q_p associated with low P_o and short τ. The dependence of the fall time on $P_{\rm rf}$ and f can be seen in Figs. 6 and 7. In Fig. 6, the total fall time for the higher power $P_{\rm rf} = 180$ W, $f = 300$ MHz data is 11 μs, while the total fall time is 17 μs for the lower 15.5-W curve in the same figure. In Fig. 7, the total fall time when $f = 250$ MHz and $P_{\rm rf} = 2$ W is 37 μs, as compared to 22 μs for the 2-MHz curve in the same figure. The total fall time for the PIPINS used in [3] made from diodes fabricated by

M/A-COM,[2] was two to three times longer than the data presented in this paper. These PIPINS had a measured $\eta_t = 0.3$, and $\tau = 4.7$ μs derived from low $P_{\rm rf}$ IL data similar to that of Fig. 4. From (1), Q_p depends on the product of the device parameters η_t and τ. At high optical power, this product is $\approx$1.5 times larger for the PIPINS of [3] compared to the Metelics PIPINS used in this paper, consistent with the longer total fall times for the former.

It can be concluded that more RF sweep out will result in a faster turn-off process; however, the value of $Q_p/(Q_s/2)$ does not completely determine the fall time since turning off the PIPINS involves the diode characteristics themselves, which are not photoconductive. It is interesting that the fall time of a series PIPINS can be much greater than τ. Charge storage and sweep out dynamics, diode characteristics, charge injection at device interfaces, charge trapping both surface and bulk, and separation of electrons and holes in the presence of a RF electric field likely play a role in the long fall times of the PIPINS. Further study is required to quantitatively understand the mechanisms that govern the fall time in these devices.

Fast fall-time switches are linked with short carrier lifetimes. Since long τ is required for the low-loss operation of a PIPINS, achieving fast fall times at the device level is problematic. Faster fall times can be achieved at the circuit level by using a series-shunt switch, as is shown in Fig. 8, where the fall time measured from 90% to 10% is 2.5 μs. The series-shunt configuration also has the advantage of greatly improved isolation, but only can be done in cases where there is a ground plane present, and is done at the cost of increased IL due to the capacitance of the shunt switch, and increasing the optical power requirement.

B. Latch-On

In the hot-switching mode, during the on–off transitions, the power dissipated in the PIPINS is greater than either the low resistance on state or the reflective off state. As a result, the maximum $P_{\rm rf}$ that the PIPINS can handle is less than that obtained for steady-state measurements. The maximum $P_{\rm rf}$ that a PIPINS can handle in hot-switching mode is limited by a latch-on effect, where $P_{\rm latch}$ is dependent on several parameters including P_o, T, and the duty cycle $d = t_{\rm on}/T$. In Fig. 9, $P_{\rm latch}$ is plotted as a function of the repetition period T, where $t_{\rm on}$ is varied to maintain $d = 50\%$. The data shows a maximum latch-on power level of 107 W when the repetition period is 10 ms. At shorter repetition periods, the $P_{\rm latch}$ level decreases. This is the result of resistive heating during the frequent switching transitions and the long fall times that results in the PIPINS remaining on well into the off-state period when T is small. At longer repetition periods, a small decrease in $P_{\rm latch}$ is observed, likely due to heating during the relatively long on periods. The data in Fig. 9 can be compared to the 180-W hot-switching data in Fig. 6 with $d = 50$ μs/30 ms $= 0.17\%$. In this case, the low duty cycle and short $t_{\rm on}$ enabled higher power operation without latch-on. The onset of latch-on has been observed to be a relatively slow process, e.g., at $P_{\rm latch}$, the tail of the RF envelope begins to grow and may take several seconds before the devices is fully latched on. It is observed that latch-on in PIPINS results in irreversible damage to the device when the latch-on state is maintained for longer than a few seconds. The damage is manifested by decreasing $P_{\rm latch}$ and increasing IL. The values of $P_{\rm latch}$ for the diodes studied here were significantly greater than $P_{\rm latch}$ for the PIPINS in [3], where $P_{\rm latch} \simeq 20$ W at low duty cycle was observed. The lower $P_{\rm latch}$ can be attributed to the smaller mesa diameter (300 μm, as compared to 760 μm) resulting in higher current density in those PIPINS. In addition, self-turn-on was observed for those PIPINS at $<$200 W.

The latch-on effect has been studied in high pulse power III–V photoconductive switches [12]–[14]. Much of the interest in latch-on with high pulse power III–V photoconductive switches is to take advantage of the effect to achieve a high gain device (where gain in this context is the ratio of electrical energy transferred to the load to the optical trigger energy). Avalanche carrier generation has been suggested as the mechanism for latch-on in GaAs photoconductive switches [13]. Silicon photoconductive switches have also been studied for high pulse power applications though latch-on is not observed in the silicon devices [13].

In measurements performed here, latch-on is observed in RF-biased silicon-based PIPINS with periodic optical pulsing. The dependency of $P_{\rm latch}$ on repetition period, duty cycle, and diode mesa diameter, and the slow onset of latch-on are consistent with thermal effects being responsible for latch-on. Because of the complex charge carrier dynamics in these devices, charge injection and displacement currents may also play a role in the latch-on effect.

IV. Conclusion

The measurements performed show that proper PIPINS operation is consistent with a photoconductive model, where the photo-injected charge is much greater than the RF sweep out charge. The results show that PIPINS can be utilized for high-power RF switching applications. For application that do not require hot switching, the IL and standoff measurements show that PIPINS can operate up to at least 200-W RF power. For applications that require hot switching, 180-W RF power switching at low repetition rate and duty cycle has been demonstrated, though the maximum RF power level is limited by a latch-on effect, and can be significantly less at higher repetition rate and duty cycle. These high RF power results were obtained using 650-mW optical control power, representing a significant power gain. The IL of PIPINS with double the intrinsic layer thickness show only a moderate increase in IL, due to longer carrier lifetimes for larger diodes resulting from reduced surface recombination. Scaling up the size of the PIPINS will allow for even higher RF power switching at the expense of higher optical control power. The PIPINS have rise times limited by the rise time of the optical control signal. Long fall times, much greater than the charge carrier lifetime, are associated with charge storage much greater than charge sweep out.

Acknowledgment

The authors would like to thank R. Nguyen and K. Nguyen, for preparing PIPINS samples, and R. Hunt for his comments.

[2]The diodes used for [3] were M/A-COM model MA4P506-131.

REFERENCES

[1] R. C. Dempsey and R. M. Bevensee, "The synaptic antenna for reconfigurable array application—Description," in *Int. IEEE Antennas Propag. Symp. Dig.*, vol. 2, 1989, pp. 760–764.

[2] J. L. Freeman, B. J. Lamberty, and G. S. Andrews, "Optoelectronically reconfigurable monopole antenna," *Electron. Lett.*, vol. 28, pp. 1502–1503, 1992.

[3] C. K. Sun, R. Nguyen, D. J. Albares, and C. T. Chang, "Photo-injection back-to-back PIN switch for RF control," *Electron. Lett.*, vol. 33, p. 1579, 1997.

[4] J. L. Freeman, S. Ray, D. L. West, and A. G. Thompson, "Optoelectronic devices for unbiased microwave switching," in *IEEE MTT-S Int. Microwave Symp. Dig.*, 1992, pp. 673–676.

[5] C. K. Sun, R. Nguyen, C. T. Chang, and D. J. Albares, "Photovoltaic-FET for optoelectronic RF/μwave switching," *IEEE Trans. Microwave Theory Tech.*, vol. 44, pp. 1747–1750, Oct. 1996.

[6] A. Rosen, P. Stabile, W. Janton, A. Gombar, P. Basile, J. Delmaster, and R. Hurwitz, "Laser-activated PIN diode switch for RF application," *IEEE Trans. Microwave Theory Tech.*, vol. 37, pp. 1255–1257, Aug. 1989.

[7] C. K. Sun, C. T. Chang, R. Nguyen, and D. J. Albares, "Photovoltaic-PIN diodes for RF control—Switching application," *IEEE Trans. Microwave Theory Tech.*, vol. 47, pp. 2034–2036, Oct. 1999.

[8] P. Katzin, B. E. Bedard, M. B. Shifrin, and Y. Ayasli, "High speed, 100+ W RF switches using GaAs MMICs," *IEEE Trans. Microwave Theory Tech.*, vol. 40, pp. 1989–1995, Nov. 1992.

[9] S. M. Zse, *Physics of Semiconductor Devices*, 2nd ed. New York: Wiley, 1981, p. 749.

[10] M. Calulton, A. Rosen, P. J. Stabile, and A. Gombar, "PIN diodes for low-frequency high-power switching applications," *IEEE Trans Microwave Theory Tech.*, vol. MTT-30, pp. 875–881, June 1982.

[11] R. U. Martinelli and A. Rosen, "The effects of storage time variation on the forward resistance of silicon p^+–n–n^+ diodes at microwave frequencies," *IEEE Trans. Electron Devices*, vol. ED-27, pp. 1728–1732, Sept. 1980.

[12] A. Rosen and F. Zutavern, Eds., *High-Power Optically Activated Solid-State Switches*. Norwood, MA: Artech House, 1994, p. 260.

[13] F. J. Zutavern, G. M. Loubriel, M. W. O'Malley, L. P. Shanwald, W. D. Helgeson, D. L. McLaughlin, and B. B. McKenzie, "Photoconductive semiconductor switch experiments for pulsed power applications," *IEEE Trans. Electron Devices*, vol. 37, pp. 2472–2477, Dec. 1990.

[14] K. H. Schoenbach, J. S. Kenney, F. E. Peterkin, and R. J. Allen, "Temporal development of electric field structures in photoconductive GaAs switches," *Appl. Phys. Lett.*, vol. 63, no. 15, pp. 2100–2102, 1993.

E. W. Jacobs received the B.A. degree in physics and M.S. degree in applied physics from the University of California at San Diego, in 1981 and 1986, respectively.

Since 1981, he has been with the Space and Naval Warfare Systems Center San Diego (formerly Naval Ocean Systems Center), San Diego, CA. His research interests include properties of piezoelectric polymers, stochastic nonlinear dynamics, fractal-based image compression, and OE devices.

Mr. Jacobs is a member of the American Physical Society.

D. W. Fogliatti received the B.S. degree in physics from the University of California at Los Angeles, in 1999.

He is currently with the Applied Nonlinear Dynamics Group, Space and Naval Warfare Systems Center San Diego, San Diego, CA, where he is involved with improving detection in sensors and communication systems by applying nonlinear processing techniques.

H. Nguyen received the B.S. degree in electrical engineering from University of California at San Diego, in 1999, and is currently working toward the M.S. degree in electrical engineering at San Diego State University, San Diego, CA.

In 1999, he joined the Space and Naval Warfare Systems Center San Diego, San Diego, CA. His research interests include optical communication, communication theory, and adaptive processing.

D. J. Albares received the A.B. degree in physics from Princeton University, Princeton, NJ, in 1954, and the Ph.D. degree in physics from the University of Colorado, Boulder, in 1969.

He was involved with plasma physics at General Atomic, San Diego, CA, and was a Post-Doctoral Fellow at the University of Southern California, Los Angeles. From 1970 to 1999, he was with the Space and Naval Warfare Systems Center San Diego (formerly Naval Ocean Systems Center), San Diego, CA, where he was involved with fiber optics, integrated optics, and optoelectronics. He is currently with the Peregrine Semiconductor Corporation, San Diego, CA, and also consults.

Dr. Albares is a member of the Optical Society of America.

C. T. Chang (S'73–M'75) received the B.S. degree in physics from the National Taiwan Normal University, Taiwan, R.O.C., in 1966, the M.S. degree in physics from North Dakota State University, Fargo, in 1969, and the Ph.D. degree in electrical engineering from the University of Washington, Seattle, in 1975.

From 1975 to 1977, he was a Research Associate with the University of Washington, where he conducted research in optical holography and fiber optics. In 1977, he joined the Space and Naval Warfare Systems Center San Diego (formerly Naval Ocean Systems Center), San Diego, CA. In 1979, he joined San Diego State University, San Diego, CA, where he is currently a Professor of electrical and computer engineering. His research interests are optical-fiber communications and optoelectronics.

C. K. Sun received the B.S. degree in electro-physics from the National Chiao Tung University, Taiwan, R.O.C., in 1983, and the Ph.D. degree in electrical engineering from the University of California at San Diego, in 1993.

From 1992 to 2000, he was with the Space and Naval Warfare Systems Center San Diego, San Diego, CA, where his interests were optics and optoelectronics. He is currently with Lightwave Solutions Inc., San Diego, CA, where his research interests include electroabsorption modulators and their application to fiber-optic communications links.